Geochemistry Geophysics Geosystems G3
AN ELECTRONIC JOURNAL OF THE EARTH SCIENCES
Published by AGU and the Geochemical Society

Article
Volume 9, Number 10
7 October 2008
Q10006, doi:10.1029/2008GC002156
ISSN: 1525-2027

Halogen and ^{129}I systematics in gas hydrate fields at the northern Cascadia margin (IODP Expedition 311): Insights from numerical modeling

Zunli Lu
Department of Earth and Environmental Sciences, 227 Hutchison Hall, University of Rochester, Rochester, New York 14627, USA

Now at Earth Sciences, University of Oxford, Parks Road, Oxford OX1 3PR, UK (zunli.lu@earth.ox.ac.uk)

Christian Hensen
Leibniz-Institut für Meereswissenschaften, IFM-GEOMAR, Wischhofstr. 1-3, D-24148 Kiel, Germany

Udo Fehn
Department of Earth and Environmental Sciences, 227 Hutchison Hall, University of Rochester, Rochester, New York 14627, USA

Klaus Wallmann
Leibniz-Institut für Meereswissenschaften, IFM-GEOMAR, Wischhofstr. 1-3, D-24148 Kiel, Germany

[1] We measured halogen concentrations and $^{129}I/I$ ratios in five drilling sites of Integrated Ocean Drilling Program Expedition 311 (offshore Vancouver Island, Canada) in order to identify potential sources of fluids and methane in gas hydrate fields. Iodine is dominated by organic decomposition and transports with fluids in reducing environments and the presence of the cosmogenic radioisotope ^{129}I ($T_{1/2}$ = 15.7 Ma) allows the age determination of organic sources for iodine. Here we report halogen concentrations in 135 pore water samples, I concentrations in 48 sediment samples, and $^{129}I/I$ ratios measured in a subset of 20 pore water samples. Most $^{129}I/I$ ratios fall into a range around 500×10^{-15}, corresponding to a minimum age of 25 Ma and the lowest ratio of 188×10^{-15} (T_{min} = 47 Ma) was observed at 208 m below sea floor (mbsf) in Site 1326. These ages are considerably older than that of the local sediments in the gas hydrate fields and that of the subducting sediments on the Juan de Fuca plate, indicating that old, accreted sediments in the accretionary wedge contribute a significant amount of iodide and, by association, of methane to the gas hydrate occurrences. A geochemical transport-reaction model was applied to simulate the advection of deeply sourced fluids and the release of iodide, bromide, and ammonia in the host sediments due to organic matter degradation. The model was first tested with data from two well studied areas, Ocean Drilling Program Site 1230 (Peru margin) and Site 1245 (Hydrate Ridge). The model results for the Expedition 311 sites indicate that the in situ release of young iodine is relatively minor in comparison to the contribution of migrating fluids, carrying large amounts of old iodine from deep sources. The comparison between the sites demonstrates that the total organic content has a strong effect on the rate of in situ iodine release and that lateral flows along fractures can have a significant influence on pore water chemistry, especially at the Cascadia margin. The iodine results indicate that mobilization and transport of methane from sources in the upper plate of active margins is an important process which can also play a substantial role in the formation of gas hydrate fields.

Components: 9273 words, 7 figures, 4 tables.

Keywords: halogen; ^{129}I/I ratio; gas hydrate; IODP Expedition 311; numerical modeling.

Index Terms: 3610 Mineralogy and Petrology: Geochemical modeling (1009, 8410); 1031 Geochemistry: Subduction zone processes (3060, 3613, 8170, 8413); 3004 Marine Geology and Geophysics: Gas and hydrate systems.

Received 5 July 2008; **Revised** 25 August 2008; **Accepted** 28 August 2008; **Published** 7 October 2008.

Lu, Z., C. Hensen, U. Fehn, and K. Wallmann (2008), Halogen and ^{129}I systematics in gas hydrate fields at the northern Cascadia margin (IODP Expedition 311): Insights from numerical modeling, *Geochem. Geophys. Geosyst.*, *9*, Q10006, doi:10.1029/2008GC002156.

1. Introduction

[2] Fluid flow at subduction zones plays an important role in global geochemical budgets and mechanical properties of the sedimentary wedge [*Kastner et al.*, 1991; *Saffer and Bekins*, 1999]. Fluids are released from compaction of porous sediments at shallow levels and from diagenetic reactions such as clay mineral dehydration at great depths [*Bekins et al.*, 1995]. Marine gas hydrates have been commonly recovered along continental margins associated with the seepage of fluids chemically distinct from seawater [*Kastner et al.*, 1991]. The formation of gas hydrates relies on the methane produced from degradation of organic matters, which can be produced locally or transported by fluids which travel along conduits like decollement, faults, and fractures. Many investigations are focused on sources, diagenetic processes, and fluid pathways by studying the methane-rich fluids with various geochemical parameters in forearc regions, such as Li, Sr, B, O, Cl, Br, and I [*Chan and Kastner*, 2000; *Kastner et al.*, 1995; *Martin et al.*, 1991; *Martin et al.*, 1993; *Teichert et al.*, 2005; *Torres et al.*, 2004a].

[3] Among these tracers, the iodine system provides unique insights into the fluids associated with organic matter decomposition, due to its strong biophilic nature [*Kennedy and Elderfield*, 1987; *Ullman and Aller*, 1983] and the presence of the radioactive isotope ^{129}I. ^{129}I/I ratios measured in pore waters can be used to calculate the age of organic materials releasing iodide and other degradation products [*Fehn et al.*, 2000; *Tomaru et al.*, 2007b]. This tool is particularly useful to identify organic sources at forearc areas where fluids mix and migrate over long distances through a series of geologic units with different ages [*Fehn et al.*, 2003; *Fehn et al.*, 2006]. A common observation from these investigations is that a major fraction of iodide in the pore water is carried in by fluid advection rather than local production from host sediments, which is consistent with the very low percentage of iodine partitioning into the solid phase [*Muramatsu et al.*, 2007]. By implication, as iodine is transported within fluids, other decomposition products such as methane will also be transported, thereby delivering methane to loci higher within the sedimentary column where gas hydrate can form.

[4] In combination with geochemical analyses, numerical models have also been applied to investigate the origin of methane in gas hydrates, as, for example, at Hydrate Ridge [*Torres et al.*, 2004b], Costa Rica [*Hensen and Wallmann*, 2005], and Blake Ridge [*Davie and Buffett*, 2003; *Wallmann et al.*, 2006]. We developed a transport-reaction model of this type to quantify the contribution of iodine from different organic sources. The model was first calibrated by sites at the Peru Margin and Hydrate Ridge and then applied to the sites investigated in this study. In this paper, we present new data of halogen concentrations in pore waters, ^{129}I/I ratios in pore waters, and iodide concentrations in sediments from northern Cascadia margin, in combination with modeling results to discuss potential sources of methane and fluids. All of the samples were collected by the Integrated Ocean Drilling Program (IODP) during Expedition (Exp) 311 in the fall of 2005.

2. Geologic Setting

[5] Cascadia margin, along the west coast of the United States and Canada, has been the target of many investigations about gas hydrates. Two prime examples in this area include Hydrate Ridge, offshore Oregon on central Cascadia margin [*Trehu et al.*, 2004] and northern Cascadia offshore Vancouver Island [*Lu et al.*, 2007a; *Pohlman et al.*, 2005]. The drilling sites of IODP Exp 311 are

located on the accretionary prism of the northern Cascadia subduction zone, southwest of Vancouver Island. The Juan de Fuca Plate currently converges with the North American Plate at a rate of ~45 mm/a [*Jarrard*, 1986] (Figure 1a). The age of the Juan de Fuca Plate near the southern Vancouver Island is between 2 and 8 Ma [*Davis and Hyndman*, 1989]. The incoming sediment pack consists of a fine-grained pre-Pleistocene hemipelagic section and an overlying Pleistocene turbidite section. Landward to the deformation front is an accretionary wedge up to 100 km wide formed by scraping the sediments off the subducting slab since Eocene time (Figure 1b). The Crescent Terrane, a 52–57 Ma old oceanic igneous formation, has been emplaced onto the upper plate and provided a backstop to the large sedimentary prism since 42 Ma [*Hyndman et al.*, 1990]. Further eastward, the Pacific Rim Terrane is composed of Mesozoic sedimentary rocks, outcropping along the south and west coast of Vancouver Island. It was accreted to the North America Plate in the same plate reorganization event as the Crescent Terrane [*Hyndman et al.*, 1994]. The forearc Tofino basin, up to 4 km deep, covers most of the accreted terrane and sedimentary wedge. The basin was initially formed by rapid subsidence associated with the deposition of deep marine sediments from Eocene to Holocene with a recent tendency to shallow water depth. The Tertiary sedimentary sequence is comprised of marine conglomerates, sandstones, and shales [*Hyndman et al.*, 1990].

[6] In the study area (Figure 1a), a margin-perpendicular transect (U1326, U1327 and U1329) was drilled landward from an uplifted ridge close to the deformation front. Water depth decreases from ~1828 m at U1326 to ~946 m at U1329. Site U1325 is located eastward of the ridge in a slope basin, with a relatively flat seafloor and a depth of ~2200 m. Site U1328 represents an active cold vent related to focused fluid flows, distinctive from the other sites. We report here results of pore water and sediment samples from all five sites. Bottom seismic reflectors (BSRs) have been widely observed across the northern Cascadia margin and were used to map the general distribution of gas hydrates in Figure 1a [*Riedel et al.*, 2006]. BSRs were found in these sites generally between 200 and 250 mbsf, but at a more shallow depth of 125 mbsf at Site 1329.

3. Halogen and ^{129}I System

[7] Iodine is the most biophilic element among the halogens and its geochemical behavior is very different from chlorine, which usually is not associated with organic matter. Bromine has characteristics somewhat between the other two elements and is commonly examined together with I and Cl. Seawater is the largest surface reservoir of Cl, but marine sediments are the dominant pool of iodine [*Muramatsu and Wedepohl*, 1998]. It is a result of the extensive enrichment of I in marine phytoplankton and algae compared to seawater and its subsequent accumulation in marine sediments [*Elderfield and Truesdale*, 1980]. Halogens in pore fluids are useful indicators for diagenetic processes at subduction zones. Fluids with low chloride concentrations are commonly associated with clay dehydration or gas hydrate dissociation [*Kastner et al.*, 1991], while fluids in hydrate fields are highly enriched in iodide, a strong indication of organic matter degradation. Because iodide and methane are released from organic sources and transported along with fluids, halogen concentrations and iodine ages determined in combination can help unravel the location and age of the source region for fluids and methane.

[8] Iodine has one stable isotope ^{127}I and one cosmogenic radioisotope ^{129}I. The long-lived ^{129}I, with a half-life of 15.7 million years, allows age determinations up to 80 Ma. It is produced by the interaction of cosmic rays with xenon isotopes in the atmosphere (cosmogenic ^{129}I) and the spontaneous fission of ^{238}U in the crust (fissiogenic ^{129}I). Both of these mechanisms contribute at similar rates to the total amount of natural ^{129}I [*Fabryka-Martin et al.*, 1985]. Iodine is well-mixed in surface reservoirs, including the oceans and shallow sediments. The preanthropogenic ^{129}I/I ratio in recent marine sediments is $^{129}I/I_{init} = (1500 \pm 150) \times 10^{-15}$, and this input ratio is used for age determinations in the marine system [*Fehn et al.*, 2007a]. Large quantities of anthropogenic ^{129}I have been released from atmospheric bomb tests and the reprocessing of nuclear fuel [*Snyder and Fehn*, 2004], but anthropogenic ^{129}I typically does not reach layers deeper than 50 cm in marine sediments [*Moran et al.*, 1998]. The only method, capable of measuring the very low concentrations of preanthropogenic ^{129}I, is accelerator mass spectrometry (AMS). Measured ^{129}I/I ratios (R_{mes}) can be used to calculate the time (t) since iodine was buried, according to the decay equation:

$$R_{mes} = R_{init} e^{-\lambda_{129} t} \quad (1)$$

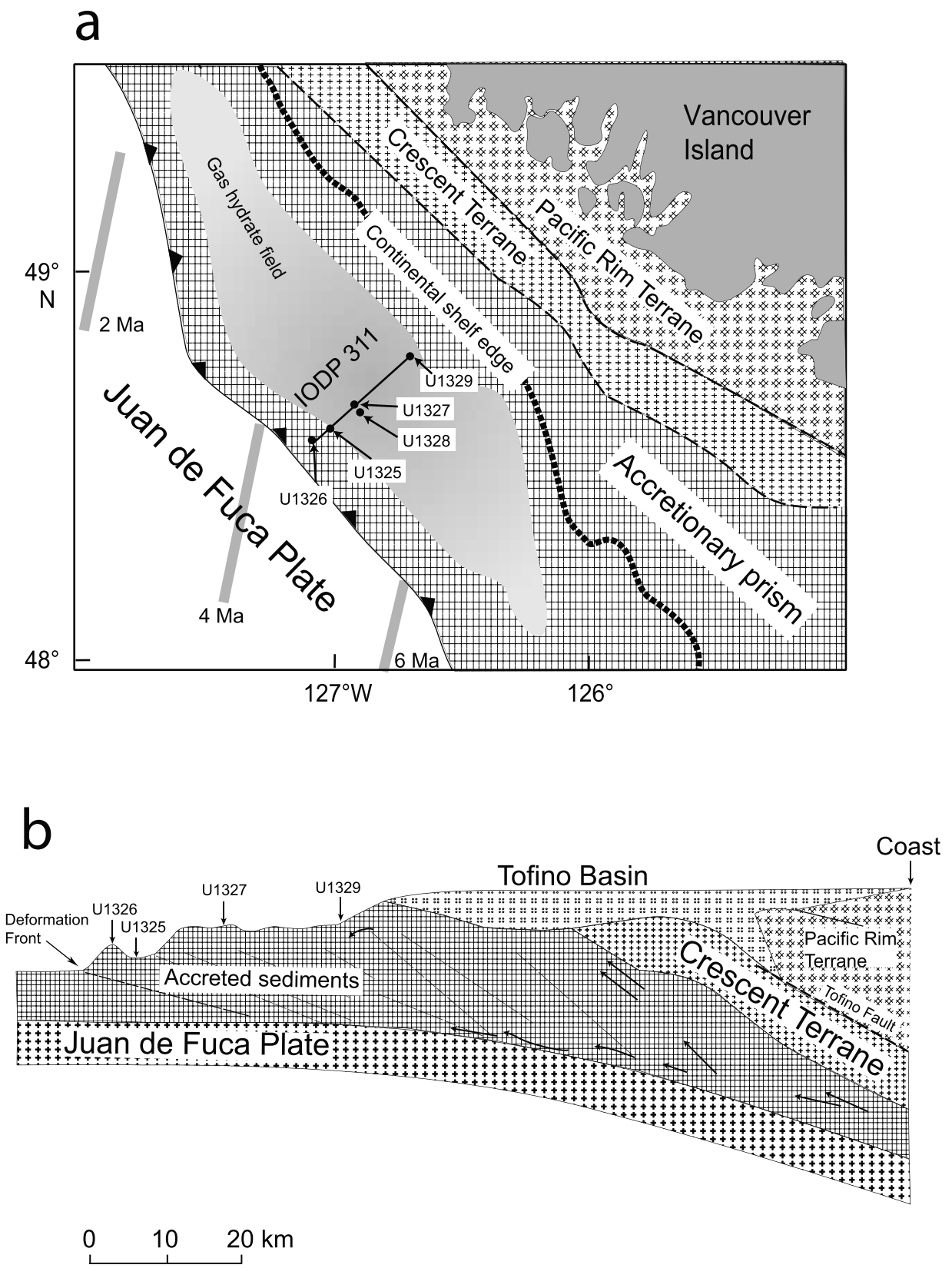

Figure 1. (a) Site map for Integrated Ocean Drilling Program (IODP) Expedition (Exp) 311; (b) A cross section of the northern Cascadia margin modified from IODP Exp 311 Preliminary Report [*Riedel et al.*, 2006] and *Hyndman et al.* [1990]. Arrows represent fluid flows and dashed lines indicate faults.

with the initial ratio of 1500×10^{-15} (R_{init}) and the decay constant of 4.4×10^{-8} a^{-1} (λ_{129}).

4. Samples and Analytical Methods

[9] We received a total of 140 pore water samples collected by Exp 311, ranging from 17 to 39 samples for each site. Pore waters were extracted from sediment cores following the standard protocol of ODP/IODP. They were sealed in air-tight glass vials preventing the iodine from oxidation and escaping. The volume of individual samples was typically around 5 ml and varied between 1 and 10 ml. Chloride and ammonia concentrations were measured shipboard [*Riedel et al.*, 2006]. We used inductively coupled plasma–mass spectrometry (Thermal X7) at the University of Rochester to determine the total iodide and bromide concentrations. The sample preparation for ICP-MS analysis followed established methods [*Muramatsu and Wedepohl*, 1998]. Every sample was measured for at least three cycles and 200 sweeps in each cycle, reaching accuracies for concentrations of better than 1%.

[10] Iodine in a selected set of pore waters were extracted, purified, and precipitated as AgI at the Rochester Cosmogenic Isotope Laboratory [*Fehn et al.*, 1992]. The iodine isotope ratios were determined at the AMS facility at PrimeLab, Purdue University [*Sharma et al.*, 2000]. The errors listed with isotope ratios are the result of variations in both the stability of the AMS system and the amount of AgI provided. An actual AMS determination usually requires 1 mg of AgI, although samples with masses as low as 0.1 mg can produce reliable ratios with diminished accuracy [*Lu et al.*, 2007b]. Adjacent pore waters were combined when not enough volume was available for a single sample.

[11] Sediments, where pore waters had been extracted shipboard (squeeze cakes), were used for the determination of sediment-bounded iodine concentrations [*Muramatsu and Wedepohl*, 1998]. They were washed with deionized water to remove residual pore waters, dried in oven over night at 60°C, ground to fine grain powders, and heated in a tube furnace to 1000°C for 30 min. An organic alkaline solution, tetramethyl ammonium hydroxide (TMAH), was used as a trap solution to receive iodine remobilized from the sediments. The typical uncertainty of this method is ~10% and is not listed in the table.

5. Numerical Modeling Approach

5.1. Model Description

[12] A Mathematica-based, one dimensional, transport-reaction model was applied to simulate the transport of deep-sourced old iodine and the in situ release of younger iodine in anoxic marine sediments. The model calculates vertical fluid flow, molecular diffusion, degradation of particulate organic carbon (POC) by sulphate reduction and methanogenesis, and radioactive decay of ^{129}I. The setup of partial differential equations for solids and solutes are almost identical to that described by *Hensen and Wallmann* [2005], except that degradation kinetics of POC follows the simplified approach of *Wallmann et al.* [2006], where the degradation is basically decreased by the buildup of reaction products (CH_4, CO_2) in pore water and the age-alteration of POC. In this simplified approach only CH_4 has been considered to have an effect on degradation kinetics:

$$R_{POC} = \frac{k_{meth}}{2 \cdot [CH_4] \cdot k_{meth}} \cdot k_x \cdot [POC] \quad (2)$$

where R_{POC} is the POC degradation rate, [CH_4] is the ambient methane concentration in pore waters, k_{meth} is a Monod constant describing the inhibition of POC degradation by CH_4, k_x is an age-dependent kinetic constant, and [POC] is the POC concentration.

[13] As NH_4, Br, and I are associated with sedimentary organic matter and concurrently released by POC degradation into ambient pore waters these rates were calculated as:

$$R_{PON} = \frac{14}{12} \cdot r\mathrm{NH_4} \cdot R_{POC} \quad (3)$$

$$R_{POB} = \frac{90}{12} \cdot r\mathrm{Br} \cdot R_{POC} \quad (4)$$

$$R_{POI} = \frac{127}{12} \cdot r\mathrm{I} \cdot R_{POC} \quad (5)$$

$$R_{POI^*} = \frac{129}{12} \cdot r\mathrm{I}^* \cdot R_{POC} \quad (6)$$

where R_{PON}, R_{POBr}, R_{POI}, and R_{POI*} are the rates of N, Br, I, and ^{129}I release by POC degradation, rNH_4, rBr, rI, and rI* are the N/C, Br/POC, I/POC, and ^{129}I/POC molar ratio in the sedimentary organic matter. POI and POBr refer to I and Br bound to POC. Concentrations of ammonia are, however, not only related to the decomposition of PON since ammonia levels in pore water are strongly affected by adsorption on sediment particles [*Mackin and Aller*, 1984; *Rosenfeld*, 1979]. The dynamics between the three N reservoirs PON, dissolved ammonia, and adsorbed nitrogen are considered in the present model following the approach developed by *Hensen and Wallmann* [2005].

5.2. Model Calibration

[14] The model was first calibrated with the data reported for ODP Site 1230 on the Peru margin [*Fehn et al.*, 2007b]. This site is known for the recovery of gas hydrates in a forearc setting similar to the sites of Exp 311. Another reason to choose this site for the preliminary calibration of the model is that all of the pore water profiles in this site show regular curvatures (Figure 2) typically observed in marine sediments. Although the measured iodide and bromide concentrations dropped between 140 and 148 mbsf, they do not show any significant deviations from the general depth trend and no variations are noticeable in chloride and ammonia concentrations at the same depth.

[15] Two model runs are made for this site. Fixed concentration boundary (Dirichlet) conditions are used for the upper and lower boundary in the first run. The lower boundary condition simulates the upward advection of deeply sourced fluids with distinct chemical compositions, while the upper boundary represents the overlying seawater. This run simulates the upward advection of old iodine mixing with locally released young iodine by POC degradation. The input parameters are adjusted for the modeled curve to match the analytical data (Table 1). The modeled depth trends fit well with the analytical data for all of the pore water species in this run (Figure 2). The second run inherited the preferred parameter setting from the previous run, while a zero gradient (Neumann) condition has been chosen for the lower boundary. Results from this run show the pore water compositions at the same sedimentary environment without the influence of deep fluids, or in other words, the in situ production of organic species due to POC degradation within the modeled depth interval. Because POI and POBr data from this site were not available, we used data from the adjacent DSDP Site 685 [*Martin et al.*, 1993], since the variation in POI concentrations in the same area is usually found to be small in this study and other margins [*Muramatsu et al.*, 2007]. An I/C ratio of 3×10^{-4} is used to fit the measured POI concentrations (Figure 2), which is relatively high compared to the average ratio in marine plankton of 1.4×10^{-4} [*Elderfield and Truesdale*, 1980].

5.3. Sensitivity Analysis

[16] A series of sensitivity tests is applied to Site 1230 to investigate the influence of several major parameters to the chemistry of sediments and fluids. These tests are based on the best fit of the first model run. During each individual test, the parameter being analyzed was set to values over a broad range to produce a suite of modeled curves, while other parameters are fixed to the preferred value. Here we show results of varying two parameters (total organic carbon (TOC) level and flow rate) with strong influence on the halogens. The complete sensitivity tests can be obtained from the corresponding author [*Lu*, 2008].

[17] TOC level shows a strong effect to both the in situ production of iodine and the shape of the ^{129}I/I profile (Figure 2). As the initial TOC content at the seafloor were manually dropped from 3.2% to 1.5 and 0.5%, the amount of iodide released within the host sediments decreased accordingly. The ^{129}I/I ratios are observed to systematically increase toward the seafloor within the upper 100 mbsf at Site 1230. However, decreasing the TOC input also caused old iodine ages being observed in very shallow depth.

[18] The flow rate at this site was increased from 0.008 to 0.1 cm/a (Figure 3), and the most noticeable change is that the pore water composition quickly switched from seawater composition to that of deep fluids within the upper 100 mbsf. A pronounced maximum is observed in bromide and ammonia concentrations around 100 mbsf under high flow rates, whereas even a flow rate value as high as 0.1 cm/a does not produce a maximum (or peak) in iodide concentrations, below which the concentration decreases as shown in other sites (Sites 1245 in following discussion). ^{129}I/I ratio is found to decrease very quickly in the upper 25 mbsf under a fast upward flow. Chloride appears to be not very sensitive to the flow rate in this site because of the low concentration gradient and relatively scattered data points, however, it is a very good constraint for the determination of

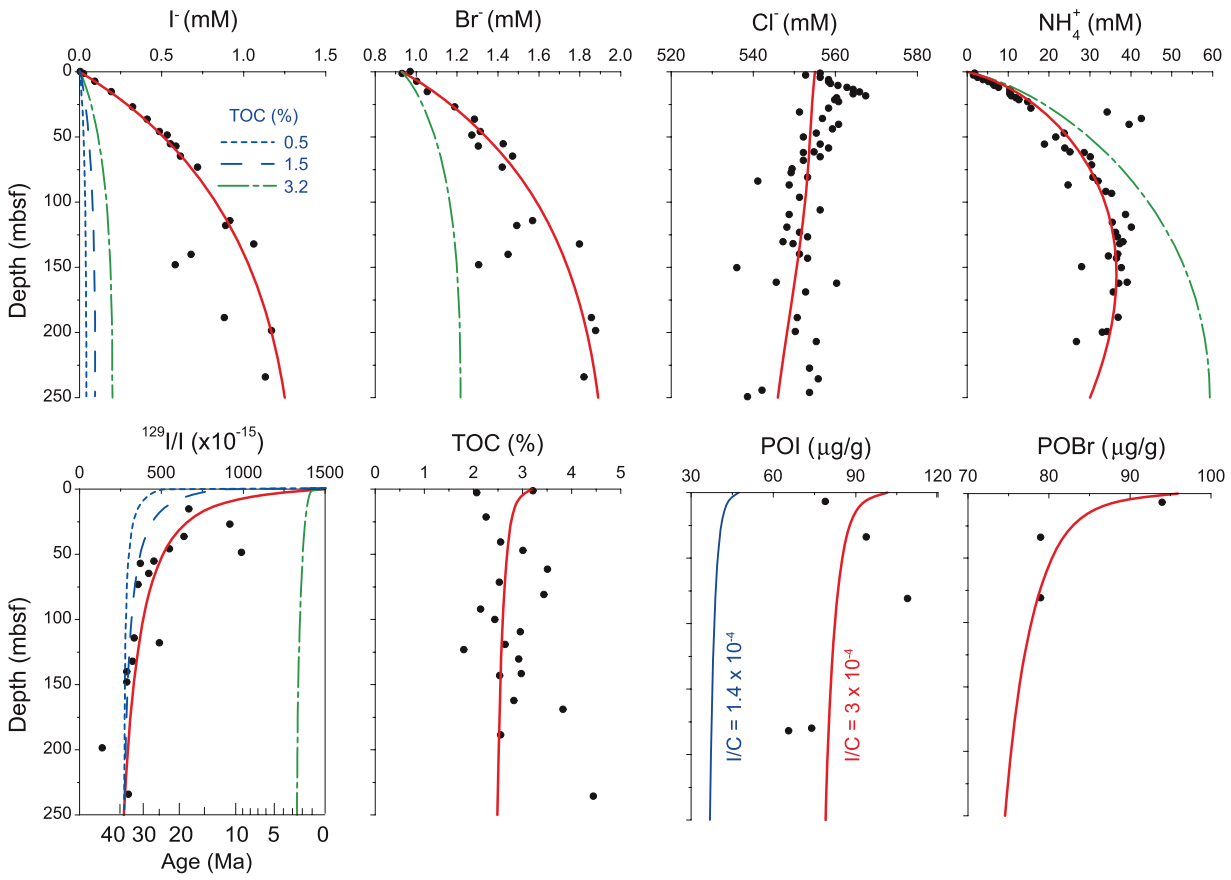

Figure 2. Modeling results of Site 1230 (Peru Margin). Thick solid lines (red) are modeled with fixed lower boundary condition and the dash-dotted lines (green) show the local iodine release calculated with open lower boundary. The thin dashed lines (blue) show the decrease in local iodine release and change as the total organic carbon (TOC) input drops from 3.2% (green dash-dotted line) to 1.5% and 0.5%. The thin solid line of particulate organic iodine (POI) concentration indicates the POI calculated with I/C ratio of 1.4×10^{-4}, significantly lower than the measured values.

flow rates at other sites where higher concentration gradients prevail.

5.4. Modeling Lateral Flows at Hydrate Ridge

[19] Hydrate Ridge is located on central Cascadia margin, offshore Oregon. It is a prime example of a marine gas hydrate field that has been well investigated recently [*Teichert et al.*, 2005; *Tomaru et al.*, 2006; *Torres et al.*, 2004a, 2004b; *Trehu et al.*, 2004]. A detailed study of the iodine system is available in association with the fluid flows in this area [*Lu et al.*, 2008]. Here we apply this new model to Site 1245, where the highest reported pore water iodide concentrations are found. In the previous study [*Lu et al.*, 2008], it has been reported that the maximum in pore water iodide concentrations (~100 mbsf) corresponds to the presence of a major fracture zone (Figure 4). The sensitivity test applied to Site 1230 also shows that the iodide maximum cannot be explained by high flow rates, sedimentation rates or strong in situ production [*Lu*, 2008]. The model setup for Site 1230 failed to reproduce the measured concentration maximum (Figure 4). These observations indicate that the fractures very likely are carrying fluids with distinct chemical compositions [*Hensen and Wallmann*, 2005], especially high iodide concentrations.

[20] Lateral fluid conduits were installed in the second run following established methods [*Hensen and Wallmann*, 2005] to simulate the influence of fractures. The identified fracture zones [*Weinberger and Brown*, 2006] were used to constrain the depth of the lateral flows (Figure 4). A Gauss-type rate

Table 1. Parameter Settings Used for the Model

Site	1325	1326	1327	1328	1329	1245	1230
Length of the sediment column (cm)	30000	27000	30000	30100	20200	40000	25000
Maximum simulation time (year)	8.00E+06	8.00E+06	8.00E+06	8.00E+06	8.00E+06	8.00E+06	8.00E+06
Seafloor temperature (°C)	3	3	3	3	3	4	5
Temperature gradient in (°C/cm)	6.00E-04	6.00E-04	6.00E-04	6.00E-04	6.00E-04	5.30E-04	3.50E-04
Water depth (m)	2200	1828	1303	1267	950	1000	1000
Upward flow rate (cm/a)	0.015	0.06	0.035	0.03	0.03	0.02	0.027
Sedimentation rate at bottom of the core (cm/a)	0.012	0.01	0.01	0.012	0.008	0.008	0.015
Porosity at zero depth	0.55	0.52	0.6	0.6	0.63	0.62	0.72
Porosity at bottom of the core	0.38	0.35	0.38	0.38	0.4	0.38	0.43
Inhibition constant for POC degradation Ki (wt.%)	20	20	20	10	8	20	38
Molar iodine to carbon ratio	7.00E-05	7.00E-05	7.00E-05	7.00E-05	7.00E-05	1.40E-04	3.00E-04
Molar bromine to carbon ratio	6.00E-04	6.00E-04	6.00E-04	6.00E-04	6.00E-04	2.20E-03	4.50E-04
Upper boundary conditions for all model runs:							
I (mM)	0.0004	0.0004	0.0004	0.0004	0.0004	0.0004	0.0004
^{129}I/I($\times 10^{-15}$)	1500	1500	1500	1500		1500	1500
Br (mM)	1.00	1.00	0.95	0.95	0.90	0.9	0.86
Cl (mM)	560	560	560	570	555	560	555
NH_4 (mM)	1.00E-03	1.00E-03	1.00E-03	1.00E-03	1.00E-03	1.00E-03	1.00E-03
POC (wt.%)	0.65	0.47	0.80	0.60	0.95	1.5	3.2
Lower boundary conditions for the preferred runs (red lines):							
I (mM)	0.65	0.53	0.36	0.58	0.12	1.2	1.25
^{129}I/I($\times 10^{-15}$)	1017	415	694	466		183	271
Br (mM)	2.20	1.85	1.30	2.05	0.95	2.2	1.89
Cl (mM)	602	578	366	487	480	554	546
NH_4 (mM)	16.0	7.5	5.5	6.8	4.5	20.0	30.0

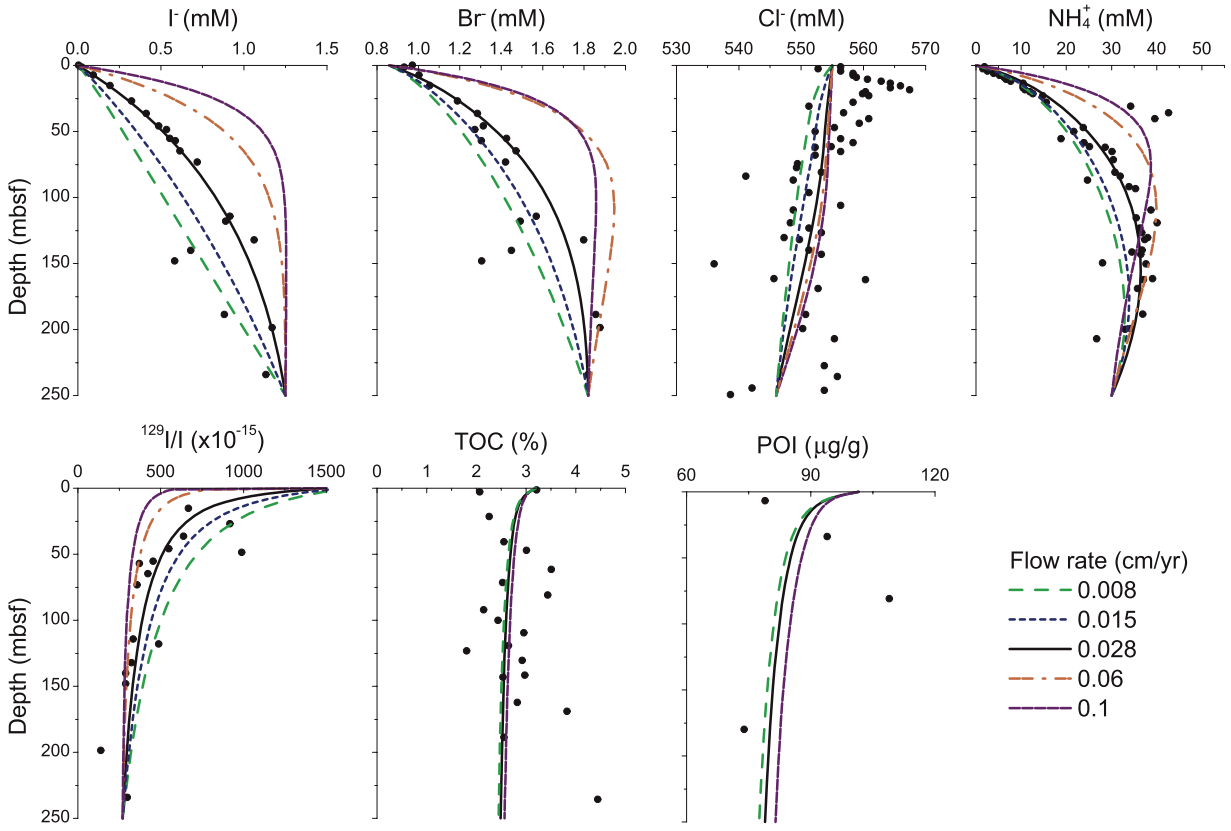

Figure 3. Sensitivity test for different flow rates.

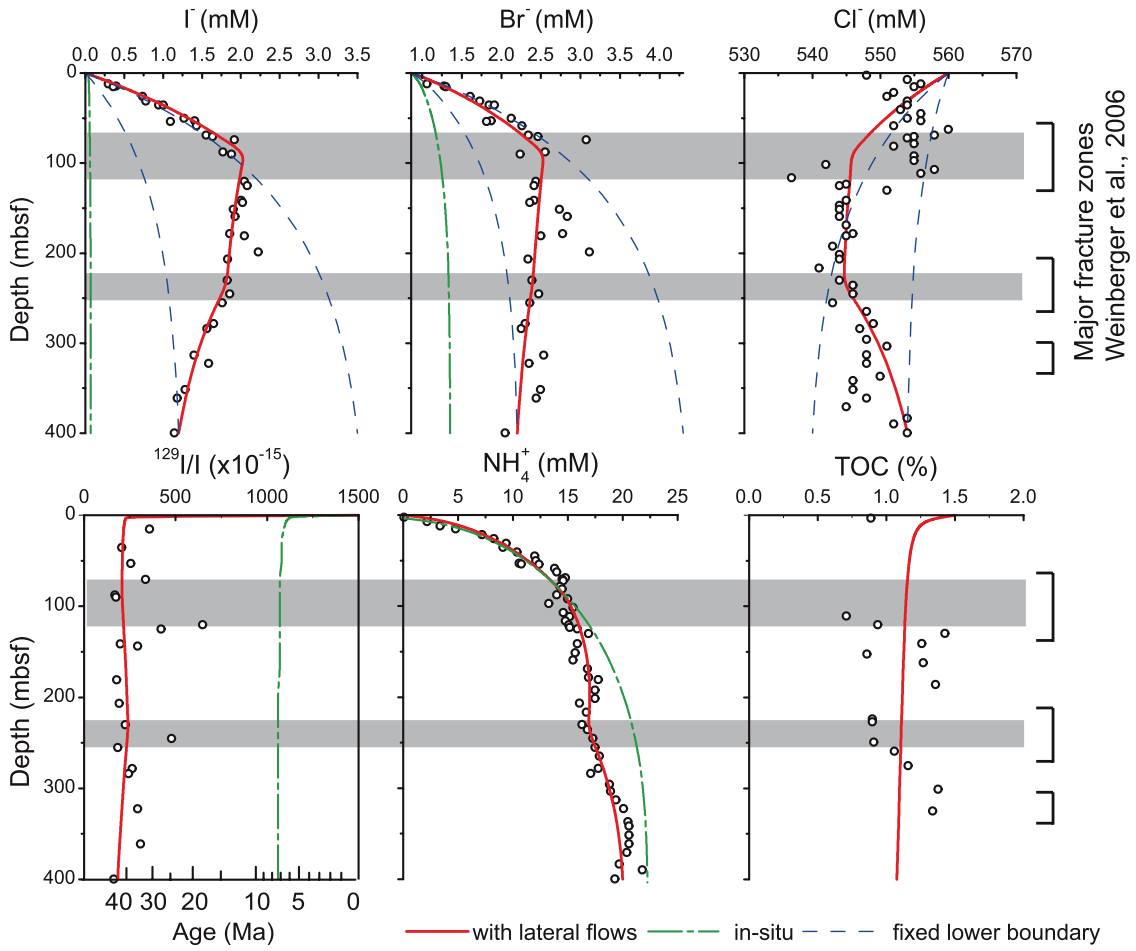

Figure 4. Modeling results for Site 1245 (Hydrate Ridge). Solid thick (red) lines show the preferred model with lateral flows, indicated by gray bars correlating with major fracture zones. The dash-dotted (green) lines are from the open lower boundary run. Two dashed (blue) lines produced with fixed lower boundary indicate that this setup cannot model the maximum/minimum in halogen concentrations.

term is calculated for the pore water species in the following form, using chloride as example:

$$R_{Cd-Cl} = ([Cl] - [Cl_{cond1}]) \cdot k_1 \cdot e^{\frac{-(x-x_1)^2}{2 \cdot w_1}} + ([Cl] - [Cl_{cond2}]) \cdot k_2 \cdot e^{\frac{-(x-x_2)^2}{2 \cdot w_2}} + .. \quad (7)$$

[Cl](x, t) − [Cl_{condi}] determines the chloride concentration difference between the conduit and the pore water, k_i is the flow intensity at conduit i in a^{-1}, x_i is the depth, and w_i is the width of the conduit i. The pore water profiles were well simulated by including lateral flows (Figure 4). An additional run was made to identify the contribution of in situ iodide release using the same method as for Site 1230 and it is calculated to be much lower than there.

6. Results (Exp 311)

6.1. Modeling the Dissolved Halogen and Ammonia Concentrations

[21] Iodide and bromide concentrations are measured in all pore waters samples. The results are listed in Table 2. Iodide concentrations in the pore waters gradually increase from the seawater value, 0.0004 mM (http://earthref.org/GERM/), to about two orders of magnitude higher at the bottom of each core (Figure 5). Along the transect from the prism toe (1326–1327–1329, Figure 1a), iodide enrichment decreases significantly toward the landward end of the hydrate field as indicated in the iodide

Table 2. Pore Water Halogen Concentrations and ^{129}I/I Ratios[a]

Site Depth (mbsf)	Br (mM)	I (mM)	Cl (mM)	^{129}I/I × 10^{-15}	± × 10^{-15}
1325					
0.7	1.02	0.06	555		
1.4	1.02	0.04	562		
1.4	1.09	0.10	565		
2.2	1.14	0.12	566		
2.4	1.12	0.08	564		
4.4	1.17	0.15	568		
5.2	1.19	0.16	570		
5.9	1.20	0.17	571	**680**	**130**
6.7	1.23	0.19	572	**680**	**130**
8.9	1.29	0.22	575		
18.2	1.53	0.34	582		
26.7	1.69	0.44	588	760	130
31.2	1.62	0.44	589	590	130
40.8	1.95	0.54	603		
45.9	1.98	0.55	605		
50.4	1.95	0.54	599	960	180
55.4	2.09	0.58	607		
66.1	2.22	0.63	607		
69.1	2.24	0.64	608		
73.0	2.15	0.63	610	253	21
105.2	2.15	0.63	606		
109.8	2.15	0.64	606		
124.2	2.26	0.65	602	560	100
128.0	2.08	0.61	613	830	140
240.9	2.15	0.59	596	**373**	**58**
249.3	2.19	0.60	593	**373**	**58**
263.3	2.22	0.61	611	1210	270
297.8	2.15	0.57	610		
1326					
0.7	1.02	0.02	566		
1.4	1.04	0.03	570		
2.2	1.07	0.05	575		
2.9	1.15	0.07	574		
6.1	1.15	0.11	574		
6.8	1.15	0.12	575		
7.6	1.16	0.13	572		
8.3	1.26	0.15	574		
9.1	1.20	0.15	572		
12.8	1.23	0.18	573		
16.3	1.34	0.23	573	**430**	**90**
19.3	1.29	0.23	574	**430**	**90**
50.8	1.49	0.35	579	750	170
188.8	1.68	0.48	545	344	36
198.9	1.82	0.49	583		
208.8	1.83	0.51	594	360	130
236.4	1.87	0.55	588		
268.5	1.99	0.57	592		
1327					
0.3	0.99	0.00	559		
0.9	0.96	0.00	557		
1.8	0.99	0.01			
2.4	0.99	0.01			
2.9	1.00	0.02			
3.2	0.98	0.02			
3.7	0.99	0.02			
4.3	1.02	0.03			
5.4	1.01	0.03			
7.5	1.04	0.05			
8.3	1.03	0.06			
15.7	1.06	0.09	532		
18.6	1.15	0.11	530		
21.6	1.15	0.12	525	**470**	**80**
24.6	1.11	0.12	522	**470**	**80**
28.0	1.11	0.13	514	**470**	**80**
32.5	1.13	0.15	506		
37.5	1.16	0.17	492		
42.0	1.22	0.18	486		
49.0	1.20	0.20	468	**770**	**130**
53.5	1.19	0.22	459	**770**	**130**
58.5	1.22	0.24	451		
63.0	1.26	0.26	443		
68.0	1.37	0.30	433		
72.5	1.31	0.29	428		
77.5	1.31	0.30	422		
80.6	1.32	0.31	421		
87.0	1.29	0.30	413		
91.5	1.43	0.35	410	600	340
105.3	1.39	0.35	404	**328**	**37**
109.0	1.38	0.35	400	**328**	**37**
114.9	1.40	0.36	400		
156.0	1.38	0.36	389		
193.6	1.31	0.34	376		
211.4	1.30	0.35	358		
224.0	1.35	0.36	371	620	350
249.9	1.34	0.37	375		
262.9	1.30	0.36	372		
1328					
0.5	0.97	0.00	557		
1.5	0.98	0.00	569		
2.3	0.99	0.00	572		
3.0	0.98	0.00	573		
4.4	0.97	0.00	569		
5.4	0.98	0.00	757		
8.0	0.97	0.00	629		
14.8	1.58	0.07	853		
17.4	1.62	0.08	859		
26.3	1.16	0.15	575		
30.9	1.28	0.19	579		
32.4	1.30	0.20	575		
38.2	1.22	0.16	511		
39.6	1.37	0.24	564		
40.2	1.32	0.21	569	**560**	**110**
43.1	1.30	0.22	571	**560**	**110**
52.9	1.36	0.25	567		
60.8	1.46	0.28	569		
78.4	1.60	0.36	566		
87.9	1.63	0.39	560	520	90
180.7	1.95	0.54	538	188	20
190.4	2.01	0.55	537		
230.9	2.13	0.58	521	427	53
298.0	2.06	0.56	501		
1329					
4.5	1.02	0.01	556		
7.5	1.00	0.02	552		

Table 2. (continued)

Site Depth (mbsf)	Br (mM)	I (mM)	Cl (mM)	$^{129}I/I \times 10^{-15}$	$\pm \times 10^{-15}$
9.6	0.96	0.02	551		
15.6	1.05	0.03	553		
17.9	0.98	0.02	549		
23.5	1.07	0.03	555		
30.0	1.03	0.03	549		
44.0	1.05	0.04	550		
53.5	1.05	0.04	549		
56.0	1.03	0.04	549		
65.0	1.06	0.06	547		
70.0	1.10	0.07	545		
74.5	1.14	0.07	544		
79.5	1.14	0.08	536		
84.0	1.16	0.09	531		
89.0	1.19	0.09	529		
98.5	1.17	0.10	527		
103.0	1.13	0.11	527		
108.0	1.12	0.10	526		
112.5	1.12	0.10	526		
119.5	1.12	0.11	515		
124.0	1.17	0.11	508		
129.0	1.17	0.12	514		
133.5	1.13	0.11	525		
138.5	1.08	0.11	525		
152.8	1.09	0.11	504		
162.5	1.04	0.12	502		

[a] Samples combined during preparation are in boldface. Here mbsf is meters below sea floor.

concentration of the deepest sample, 0.57 mM at 1326, 0.36 mM at 1327, and 0.12 mM at 1329. Iodide concentration at the basin site (1325) rapidly reaches 0.65 mM at ~67 mbsf, the highest value observed in all sites at Exp 311, and slightly decreases toward depth. This pattern is different from all other sites indicating a different fluid flow regime as expected from its distinct basin setting, even allowing for the comparatively low data coverage at Sites 1326 and 1328. The venting site (1328) shows an iodide concentration profile quite similar to 1326 reaching 0.56 mM at the bottom of this core. The bromide concentrations mimic the trend in iodide concentrations in all sites, but the enrichment in bromide is less than that of iodide.

[22] Three model runs are made for each site. Input parameters for all model runs are listed in Table 1 and the modeled curves are shown in Figure 5. The first run is performed using fixed upper and lower boundary conditions. Flow rate and concentrations at the lower boundary are adjusted to produce a reasonable fit to the observed data. The result of the first run shows a major offset between the modeled curves and the analytical data, especially in the ammonia concentrations. While the general trends in halogen concentrations are well reproduced, local variations cannot be accounted for. For chloride, we focus on the baseline trend and the freshening by gas hydrate dissociation is not modeled. With the flow rate giving reasonable fits to bromide and iodide, chloride profiles cannot be simulated without major offsets at the bottom 50–100 m. Additional offsets in modeled chloride concentrations are also observed between 30 and 80 mbsf at Site 1329. Iodide concentration in Site 1325 reaches a local maximum at ~60 mbsf. This maximum cannot be reproduced in this model run, neither can the bromide maximum nor the sharp curvature of iodide concentrations at Site 1327. Major discrepancies are observed in ammonia concentrations at all sites. The flow rate and sedimentation rate, producing relatively good fits to the halogen concentrations, lead to modeled ammonia concentrations much higher than the measured values in the entire Site 1325 and in the upper 100 to 200 mbsf at Site 1326 to 1329.

[23] The observed rough curvature of halogen and ammonia profiles is likely the result of the advection of fluids with distinct chemical composition via a number of conduits cutting through the sedimentary wedge [*Hensen and Wallmann*, 2005], as observed at Hydrate Ridge. Fluid conduits introduced in the second run significantly improve the model results and all of the dissolved species are well simulated, except that the depth resolution of ^{129}I/I ratio is not high enough to provide good constraints for the model. The number of conduits installed is kept as low as necessary to fit the halogen and ammonia data, varying between one (Site 1326) and four (Site 1329). More details about parameterization of the conduits are listed in Table 3 including depth, width, and chemical compositions.

[24] The third run is made by removing fluid conduits and opening up the lower boundary, while keeping the preferred parameter setting of the second run. This run clearly indicates that iodide released by in situ POC degradation in all of the sites only constitutes a very small fraction of the pore water iodide pool, while the majority of iodide is derived from a deep source. Similar results are found for bromide, although it is less dominated by the deep fluids.

6.2. ^{129}I/I Ratios in the Pore Waters

[25] ^{129}I/I ratios are measured in a selected subset of pore water samples (Table 2). The measured ratios range between 188 $\times$ 10^{-15} and 1210 $\times$

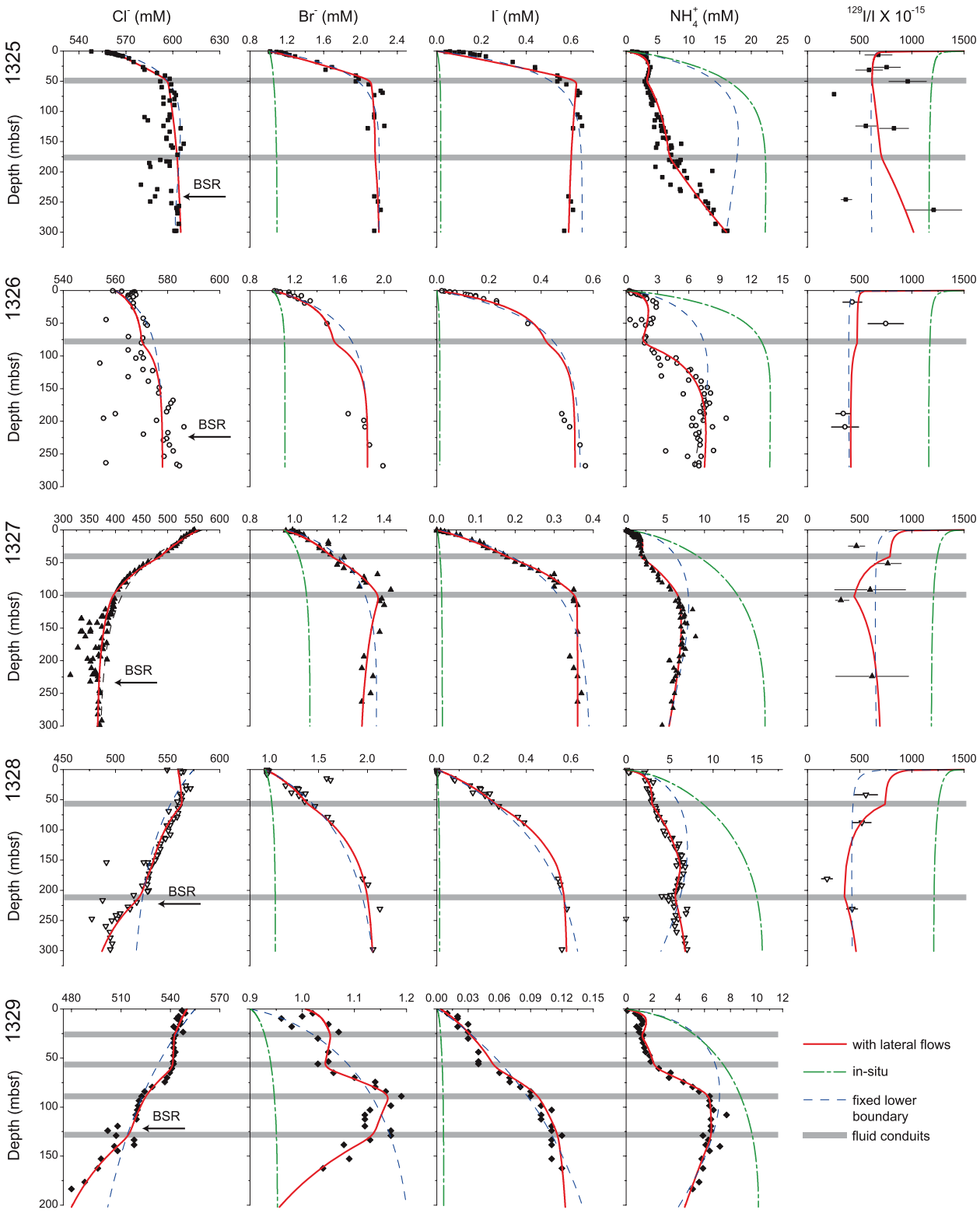

Figure 5. Halogen, ammonia concentrations, and ^{129}I/I ratios at Exp 311 Sites. Symbols are the same as in Figure 4. The disparity in Cl^- values above BSRs is due to gas hydrate dissociation. The baseline trends are used to calibrate the model.

Table 3. Chemical Composition, Flow Intensity, Depth and Width of the Conduits

Conduit	Cl (mM)	NH4 (mM)	Br (mM)	I (mM)	At (a^{-1})	Depth (cmbsf)	Width (cm)
1325–1 (51)	598	2.2	2.15	0.650	5.00E-04	4858	100
1325–2 (52)	603	6	2.15	0.600	8.00E-05	17610	100
1326–1 (61)	565	0.5	1.70	0.480	1.50E-04	8039	100
1327–1 (71)	390	7	1.40	0.370	2.00E-04	10168	100
1327–2 (72)	500	0.3	1.15	0.130	2.00E-04	4079	100
1328–1 (81)	535	6.3	1.92	0.540	1.00E-03	16047	100
1328–2 (82)	570	0.3	1.38	0.140	4.00E-05	5751	100
1328–3 (83)	525	5.5	2.00	0.570	1.00E-03	21056	100
1329–1 (91)	525	6.8	1.16	0.115	2.00E-04	12979	100
1329–2 (92)	521	6.8	1.18	0.095	6.00E-04	8716	100
1329–3 (93)	548	0.3	1.02	0.030	6.00E-04	6015	100
1329–4 (94)	543	0.7	1.05	0.030	2.00E-04	2747	100
1245–1	545	15	2.65	2.200	1.80E-04	8937	4000
1245–2	544	16.5	2.40	1.850	1.80E-04	23479	2000

10^{-15}, while the majorities are lower than 750×10^{-15} corresponding to an age range of 15–47 Ma (Figure 5). These are minimum ages because they are not corrected for the potential presence of fissiogenic ^{129}I. Estimates carried out in similar settings have demonstrated, however, that the age shift is within the machine related errors [*Fehn et al.*, 2000; *Tomaru et al.*, 2007c]. At a typical accretionary margin, iodine potentially can be released from incoming sediments on the oceanic plate, in the accretionary wedge, and the terrigenous sediments on top of the wedge. Both the sediments covering the wedge and subducting on the Juan de Fuca plate in our study area have ages younger than late Miocene and therefore cannot be responsible for the calculated iodine ages. The main source for iodine must be the old strata in the accretionary wedge, which is consistent with the results from Hydrate Ridge, located on the central part of Cascadia margin [*Fehn et al.*, 2006].

6.3. Iodine Concentrations in the Sediments

[26] Approximately 10 sediment samples were selected from each site for the determination of sediment-bound iodine (Table 4 and Figure 6). The majority of measured values fall in a range of 1–10 μg/g. The calculated I/OC molar ratios ($0.2–2.5 \times 10^{-4}$) are typical for continental margins [*Martin et al.*, 1993; *Muramatsu et al.*, 2007] and consistent with the ratios in Pacific plankton composition [*Elderfield and Truesdale*, 1980]. No systematic trend is observed either in the depth profile or along the transect (1326–1327–1329) in contrast to that seen in the pore water concentrations. The modeled POC and POI concentrations are shown in Figure 6. A uniform I/C molar ratio is applied to all sites and a value of 0.7×10^{-4} produces the best fit, which is lower than the average I/C ratio (1.4×10^{-4}) found in marine plankton [*Elderfield and Truesdale*, 1980] but similar to the ratios determined in Nankai Trough [*Muramatsu et al.*, 2007].

7. Discussion

7.1. Fluid Sources

[27] Among the halogens, iodine has the strongest biophilic nature and consequently it is most sensitive to the diagenesis of organic matter, while chloride serves as an inorganic fluid flow tracer. A plot of iodide versus chloride concentration is used to identify the influence of different sources at the studied drill sites (Figure 7). Three diagenetic sources are visible in this diagram, indicating hydrate formation, organic matter degradation, and clay dehydration. Except for hydrate formation, all other diagenetic pathways result in iodide concentrations significantly higher than seawater. Gas hydrate is considered to be rapidly forming at shallow depth in this site [*Riedel et al.*, 2006]. High chloride concentrations are measured in the upper 20 mbsf due to salt exclusion during hydrate formation at this site while influence to iodide concentration is beyond resolution of the measurements.

[28] Site 1327 and 1329 are strongly influenced by fresh water produced by clay dehydration as suggested by chloride concentrations lower than 400 mM at Site 1327 (Figure 7) [*Teichert et al.*, 2005; *Torres et al.*, 2004a]. Iodide concentrations in 1327 and 1329 are lower than those in the rest of

Table 4. Iodine Concentrations in the Sediments

Site Depth (mbsf)	I (μg/g)
1325	
40.77	10.30
72.92	12.30
89.58	2.68
132.3	4.72
156.54	5.46
190.05	3.71
210.13	3.04
252.11	1.72
297.09	2.63
1326	
2.85	5.84
42.75	2.66
70.6	2.66
103.5	2.55
121.06	1.73
156.74	7.06
188.55	1.31
219.86	2.04
244.61	3.18
268.04	2.20
1327	
3.55	2.67
41.95	1.53
62.85	7.98
80.75	6.56
128.54	2.91
155.8	3.40
191.01	6.06
215.74	8.98
272.4	9.00
291.6	6.52
1328	
2.2	6.09
38.12	1.37
71.75	11.92
101.14	14.99
127.17	2.24
150.1	7.12
180.57	2.24
219.73	6.54
241.08	5.04
278.6	2.03
1329	
2.9	1.30
26.45	0.79
64.95	1.94
98.28	5.93
125.18	2.92
152.6	6.90
183.4	6.64
201.52	1.12

the sites, likely also caused by dilution. The highest iodide concentrations in 1327 can be calculated to ~0.6 mM according to the dilution factor between their chloride concentrations and seawater. This value is similar to the highest iodide concentrations in 1326 and 1328. Sites 1325, 1326, and 1328 define a trend pointing to organic matter decomposition which produces fluids with high iodide concentrations, while the relatively low chloride concentrations indicate that Site 1328 is probably mixed with fluids freshened by clay dehydration.

7.2. Shallow Versus Deep Organic Sources for Iodine

[29] The pore water ^{129}I/I ratios clearly indicate dominantly old organic sources, located in the deep parts of the accretionary wedge, although the host sediment also contributes relatively young iodine due to in situ POC degradation. The model allows us to further evaluate the contributions from these two sources. On the basis of the pore water iodine concentrations modeled in the third run (Figure 5), only 2–5% of the iodine is released by in situ POC degradation and the rest is carried in by pore fluids, which is consistent with the observed old iodine ages.

[30] The majority of the pore water iodine ages determined in these sites are older than 10 Ma, very similar to the observations at Hydrate Ridge [*Fehn et al.*, 2006] and Nankai Trough [*Tomaru et al.*, 2007a]. The main organic source for iodine in these sites is older than the subducted sediments on the oceanic plate, indicating that the old formations within the accretionary wedge are responsible for the majority of iodine found in the shallow hydrate system.

7.3. Comparison With Hydrate Ridge and Peru Margin

[31] There is a noticeable difference in the modeled in situ iodine releasing rates among the three areas. The iodide concentration due to in situ release is calculated to be 0.007–0.021 mM at the bottom of Exp 311 sites (Figure 5), lower than the value (0.031 mM) for Site 1245 (Hydrate Ridge, Figure 4). It is likely the result of the higher TOC value of ~1.5% for Site 1245 (0.5% for Exp 311), consistent with the sensitivity analysis of Site 1230 (Figure 2). The higher I/C ratio used for Site 1245 also contributed to this difference. Because we did not receive sediment samples from this site, POI data are not available for constraining the I/C ratio. The average ratio, 1.4×10^{-4}, in marine plankton [*Elderfield and Truesdale*, 1980] is used for this site, which is twice as high as the I/C ratio used for Exp 311 sites.

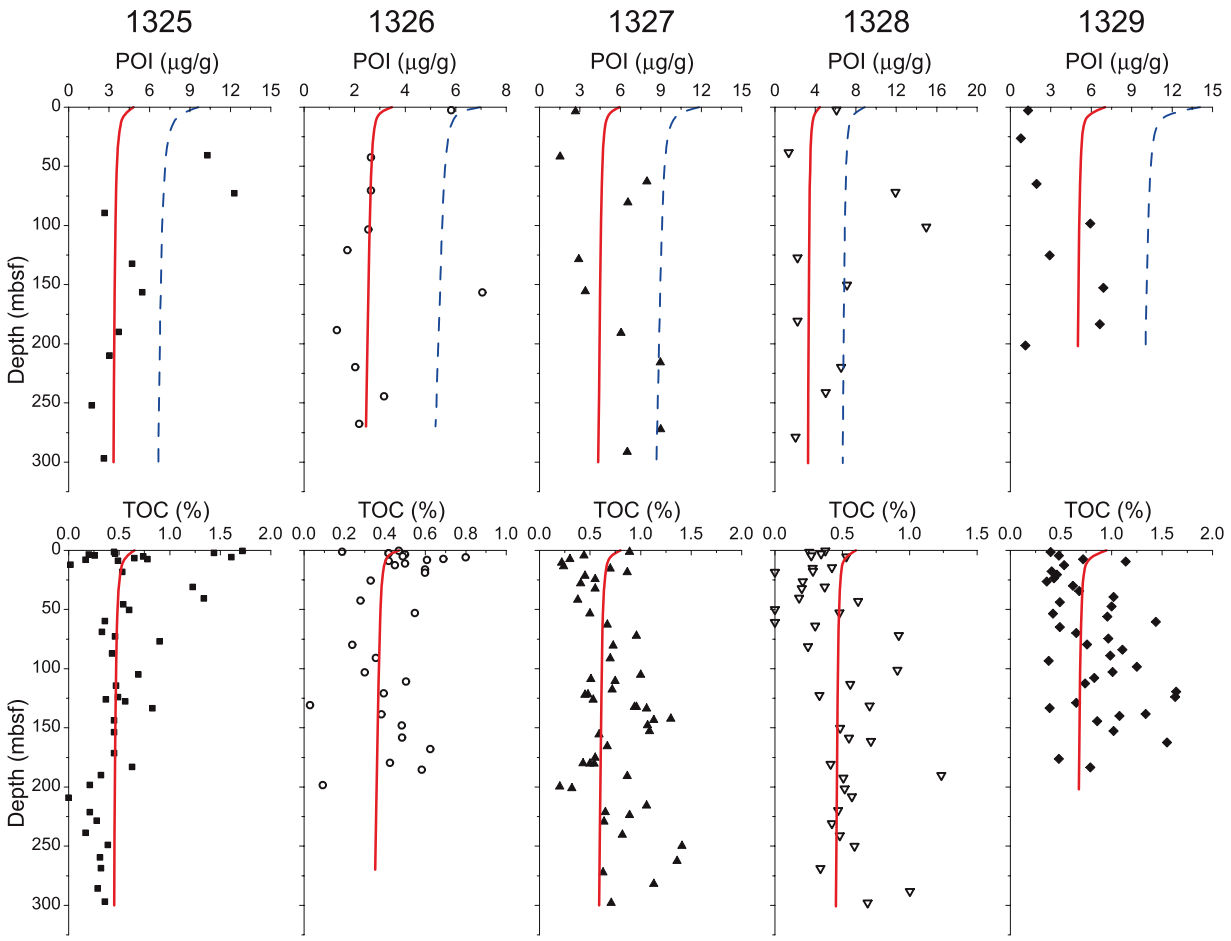

Figure 6. Iodide concentrations in the sediments and TOC. Solid curves are the modeled trends in POI and TOC. Dashed lines show an increase in I/C ratio to 1.4×10^{-4} causing overestimated residual POI.

[32] Site 1230 further demonstrates the effect of high TOC levels to the iodine pore water chemistry. TOC in this site is generally between 2 and 3%, about 2–5 times higher than the sites on Cascadia margin. As a result, the locally produced iodide at the bottom of the core constitutes 16% of the pore water iodide, much higher than that at the Cascadia margin (Figure 2). In addition to the difference in iodide releasing rate, ^{129}I/I ratios of Site 1230 gradually decrease toward depth, distinct from the ^{129}I/I profile of Site 1245, which can also be explained mainly by the different TOC level (Figure 2), although other parameters like I/C ratios, sedimentation rate and flow rate also influence the shape of the ^{129}I/I profile.

7.4. Lateral Flows

[33] Among the characteristics of the fluid conduits, the depth, chemical composition, and flow intensity play critical roles in determining the shape of modeled profiles. In order to constrain the depth of the conduits, previous applications of this approach at Costa Rica [*Hensen and Wallmann*, 2005] utilized the presence of heavy hydrocarbon gases which is known to be derived from great depth and transported with fluids. At Hydrate Ridge, the fracture distribution at Site 1245 [*Weinberger and Brown*, 2006] are consistent with the observed major changes in pore water chemistry, which also provide a good constraint on the depth of lateral flows. Although no studies at similar scale on Exp 311 sites are currently available, other geophysical investigations do suggest faults and fractures play important roles in directing fluids and changing local heat flows [*Davis and Hyndman*, 1989; *Davis et al.*, 1990; *He et al.*, 2007]. The conduits were manually assigned to the depth of strong decrease in ammonia concentration, a typical sign of deep fluids [*Hensen and Wallmann*, 2005]. Variations in ammonia concentrations are also very often associated with the irregular dipping in chloride concentrations, as observed at Sites 1328/1329. These variations in chlo-

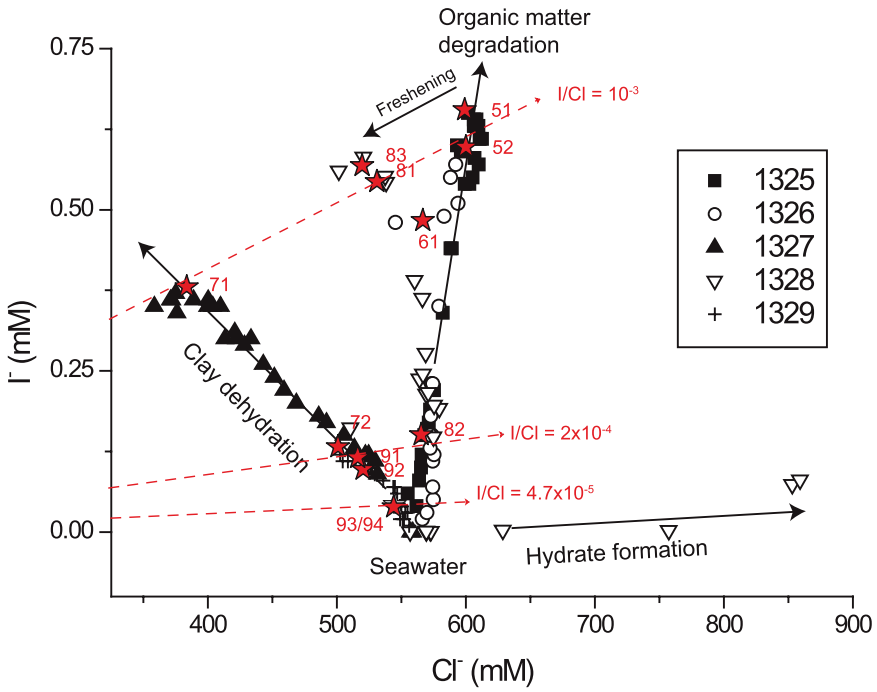

Figure 7. I versus Cl mixing plot, indicating fluid end-members and major diagenetic processes influencing the fluid chemistry. Red stars indicate the composition of fluids in the lateral conduits installed in the model, lying close to the dashed lines with constant I/Cl ratios. The shortened conduit numbers are listed in Table 3 in parentheses.

ride concentration are most likely caused by flow pattern rather than diagenetic processes, supporting the presence of fluid conduits. Although the fluid conduits and flow pattern established in the model needs to be further tested with more geochemical or hydrological data, potential modifications there should not change the conclusion that pore water iodide levels are largely controlled by lateral advection and not the local release because the low TOC level and I/C ratio in this area significantly limits the amount of in situ iodine production. It is also supported by the contrast observed between the large gradients in pore water iodine and the small variations in solid phase iodine.

[34] The model allows the chemical composition of the lateral conduits and the flow intensity to compensate for each other, which means a conduit with a very low flow intensity and a chemical composition strongly different from the ambient background might have a very similar effect to the pore water profile as a conduit with high flow intensity but less distinctive composition. No data are available to precisely constrain either parameter. Conduit concentrations are set to be within the range of reported analytical data and three groups of conduit compositions were defined by three I^-/Cl^- ratios in Exp 311 sites (Figure 7; Table 3). The flow intensity was allowed to vary in a broad range. At Site 1245 for example, an iodide concentration of 2.2 mM, the highest value reported in natural pore water, was used for the conduit to model the iodide maximum and it resulted in a flow intensity of 1.8×10^{-4} a^{-1} which is considerably higher than the value used at Costa Rica (0.8×10^{-4}) [*Hensen and Wallmann*, 2005]. Similarly strong lateral flows are also required to model rapid decreases in ammonia concentrations for Exp 311 sites.

8. Conclusions

[35] Iodide is dominated by organic material decomposition and is transported with fluids in reducing environments such as deep marine sediments. It is often strongly concentrated in the pore waters associated with gas hydrates, with enrichment factors up to a few thousands compared to seawater. The organic source of iodide very likely is also responsible for producing large amounts of methane that is ultimately delivered to the gas hydrate stability zone by fluid transport to form gas hydrates. Once iodine is released from organic matter, it migrates with fluids and is rarely involved in diagenetic processes. We applied a Mathematica-based, one-dimensional model to the drilling sites of Exp 311 at northern Cascadia

Margin, in order to simulate the transport of deep-sourced old iodine and the in situ release of younger iodine by microbial activity. In the model, iodine in the sediments is assumed to be associated only with organic materials and is released by particulate organic carbon (POC) degradation into the ambient pore waters. Depth profiles of dissolved iodide, bromide concentrations, and sediment bound iodine concentrations are calculated by the model to fit the analytical data. Modeling results suggest that the rates of POC degradation in these sediment cores can only account for a small amount of iodine (<5%), much lower than the level observed. The dominant organic source for iodine must be the deeper sediment layers. This is consistent with the old source age (~50 Ma) indicated by iodine isotope results. For comparison, we also applied the model to Site 1230, ODP 201 at Peru Margin and obtained similar results. Lateral flows play important roles in the pore water chemistry and have strong effects on the curvature of the profiles. The results demonstrate that iodine in gas hydrate locations is predominantly derived from deep, distant, and old sources with only small contributions from local organic material.

Acknowledgments

[36] This research used data provided by the Integrated Ocean Drilling Program (IODP), which is sponsored by the U.S. National Science Foundation and participating countries under management of Joint Oceanographic Institutions (JOI), Inc. We thank the crew of the JOIDES Resolution, the IODP technical staff for their support, and the onboard scientists for collecting samples. We also thank colleagues at PRIME Lab for the isotope ratio measurements. The manuscript benefited from thorough reviews by Walter Borowski and an anonymous reviewer. This work was supported by NSF OCE-050122 and by funds of the Sonderforschungsbereich (SFB) 574 at Kiel University (SFB publication 158).

References

Bekins, B. A., et al. (1995), Episodic and constant flow models for the origin of low-chloride waters in a modern accretionary complex, *Water Resour. Res.*, *31*(12), 3205–3215, doi:10.1029/95WR02569.

Chan, L. H., and M. Kastner (2000), Lithium isotopic compositions of pore fluids and sediments in the Costa Rica subduction zone: Implications for fluid processes and sediment contribution to the arc volcanoes, *Earth Planet. Sci. Lett.*, *183*(1–2), 275–290, doi:10.1016/S0012-821X(00)00275-2.

Davie, M. K., and B. A. Buffett (2003), Sources of methane for marine gas hydrate: Inferences from a comparison of observations and numerical models, *Earth Planet. Sci. Lett.*, *206*(1–2), 51–63, doi:10.1016/S0012-821X(02)01064-6.

Davis, E. E., and R. D. Hyndman (1989), Accretion and recent deformation of sediments along the Northern Cascadia Subduction Zone, *Geol. Soc. Am. Bull.*, *101*(11), 1465–1480, doi:10.1130/0016-7606(1989)101<1465:AARDOS>2.3.CO;2.

Davis, E. E., et al. (1990), Rates of fluid expulsion across the Northern Cascadia Accretionary Prism: Constraints from new heat-flow and multichannel seismic-reflection data, *J. Geophys. Res.*, *95*(B6), 8869–8889, doi:10.1029/JB095iB06p08869.

Elderfield, H., and V. W. Truesdale (1980), On the biophilic nature of iodine in seawater, *Earth Planet. Sci. Lett.*, *50*(1), 105–114, doi:10.1016/0012-821X(80)90122-3.

Fabryka-Martin, J., et al. (1985), Natural I-129 as an environmental tracer, *Geochim. Cosmochim. Acta*, *49*(2), 337–347, doi:10.1016/0016-7037(85)90027-4.

Fehn, U., et al. (1992), I-129 and Cl^{-}36 concentrations in waters of the Eastern Clear Lake area, California - Residence times and source ages of hydrothermal fluids, *Geochim. Cosmochim. Acta*, *56*(5), 2069–2079, doi:10.1016/0016-7037(92)90330-L.

Fehn, U., et al. (2000), Dating of pore waters with I-129: Relevance for the origin of marine gas hydrates, *Science*, *289*(5488), 2332–2335, doi:10.1126/science.289.5488.2332.

Fehn, U., et al. (2003), Iodine dating of pore waters associated with gas hydrates in the Nankai area, Japan, *Geology*, *31*(6), 521–524, doi:10.1130/0091-7613(2003)031<0521:IDOPWA>2.0.CO;2.

Fehn, U., et al. (2006), Data Report: 129I/I ratios and halogen concentrations in pore water of Hydrate Ridge and their relevance for the origin of gas hydrates: A progress report, *Proc. Ocean Drill. Program, Sci. Results*, *204*, 1–25.

Fehn, U., et al. (2007a), The initial 129I/I ratio and the presence of 'old' iodine in continental margins, *Nucl. Instrum. Methods Phys. Res., Sect. B*, *259*, 496–502, doi:10.1016/j.nimb.2007.01.191.

Fehn, U., et al. (2007b), Iodine as a tracer of organic material: 129I results from gas hydrate systems and fore arc fluids, *J. Geochem. Explor.*, *95*, 66–80, doi:10.1016/j.gexplo.2007.05.005.

He, T., et al. (2007), Fluid flow and origin of a carbonate mound offshore Vancouver Island: Seismic and heat flow constraints, *Mar. Geol.*, *239*(1–2), 83–98, doi:10.1016/j.margeo.2007.01.002.

Hensen, C., and K. Wallmann (2005), Methane formation at Costa Rica continental margin - Constraints for gas hydrate inventories and cross-decollement fluid flow, *Earth Planet. Sci. Lett.*, *236*(1–2), 41–60, doi:10.1016/j.epsl.2005.06.007.

Hyndman, R. D., et al. (1990), The Northern Cascadia Subduction Zone at Vancouver Island - Seismic structure and tectonic history, *Can. J. Earth Sci.*, *27*(3), 313–329.

Hyndman, R. D., et al. (1994), Regional geophysics and structural framework of the Vancouver Island margin accretionary prims, *Proc. Ocean Drill. Program, Initial Rep.*, *146*, 399–419.

Jarrard, R. D. (1986), Relations among subduction parameters, *Rev. Geophys.*, *24*(2), 217–284, doi:10.1029/RG024i002p00217.

Kastner, M., et al. (1991), Fluids in convergent margins - What do we know about their composition, origin, role in diagenesis and importance for oceanic chemical fluxes, *Philos. Trans. R. Soc. London, Ser. A*, *335*(1638), 243–259, doi:10.1098/rsta.1991.0045.

Kastner, M., et al. (1995), Geochemical evidence for fluid flow and diagenesis at the Cascadia Convergent Margin, *Proc. Ocean Drill. Program, Sci. Results*, *146*, 375–384.

Kennedy, H. A., and H. Elderfield (1987), Iodine diagenesis in non-pelagic deep-sea sediments, *Geochim. Cosmochim.*

Acta, *51*(9), 2505–2514, doi:10.1016/0016-7037(87)90301-2.

Lu, Z. (2008), Halogen and I-129 systematics in gas hydrate fields: Implications for the transport of iodine and methane in active margins, Ph.D. dissertation, Univ. of Rochester, Rochester, N. Y.

Lu, H., et al. (2007a), Complex gas hydrate from the Cascadia margin, *Nature*, *445*(7125), 303–306, doi:10.1038/nature05463.

Lu, Z., et al. (2007b), Reliability of 129I/I ratios produced from small sample masses, *Nucl. Instrum. Methods Phys. Res., Sect. B*, *259*, 359–364, doi:10.1016/j.nimb.2007.01.180.

Lu, Z., et al. (2008), Iodine ages of pore waters at Hydrate Ridge (ODP Leg 204), Cascadia Margin: Implications for sources of methane in gas hydrates, *Earth Planet. Sci. Lett.*, *267*(3–4), 654–665, doi:10.1016/j.epsl.2007.12.015.

Mackin, J. E., and R. C. Aller (1984), Ammonium adsorption in marine-sediments, *Limnol. Oceanogr.*, *29*(2), 250–257.

Martin, J. B., et al. (1991), Lithium - Sources in pore fluids of Peru Slope sediments and implications for oceanic fluxes, *Mar. Geol.*, *102*(1–4), 281–292, doi:10.1016/0025-3227(91)90012-S.

Martin, J. B., et al. (1993), Bromine and iodine in Peru Margin sediments and pore fluids - Implications for fluid origins, *Geochim. Cosmochim. Acta*, *57*(18), 4377–4389, doi:10.1016/0016-7037(93)90489-J.

Moran, J. E., et al. (1998), Variations in I-129/I-127 ratios in recent marine sediments: Evidence for a fossil organic component, *Chem. Geol.*, *152*(1–2), 193–203, doi:10.1016/S0009-2541(98)00106-5.

Muramatsu, Y., and K. H. Wedepohl (1998), The distribution of iodine in the earth's crust, *Chem. Geol.*, *147*(3–4), 201–216, doi:10.1016/S0009-2541(98)00013-8.

Muramatsu, Y., et al. (2007), Halogen concentrations in pore waters and sediments of the Nankai Trough, Japan: Implications for the origin of gas hydrates, *Appl. Geochem.*, *22*, 534–556, doi:10.1016/j.apgeochem.2006.12.015.

Pohlman, J. W., et al. (2005), The origin of thermogenic gas hydrates on the northern Cascadia Margin as inferred from isotopic (C-13/C-12 and D/H) and molecular composition of hydrate and vent gas, *Org. Geochem.*, *36*(5), 703–716, doi:10.1016/j.orggeochem.2005.01.011.

Riedel, M., et al. (2006), *Proceedings of the Integrated Ocean Drilling Program*, vol. 311, U. S. Govt. Print. Off., Washington, D. C.

Rosenfeld, J. K. (1979), Ammonium adsorption in nearshore anoxic sediments, *Limnol. Oceanogr.*, *24*(2), 356–364.

Saffer, D. M., and B. A. Bekins (1999), Fluid budgets at convergent plate margins: Implications for the extent and duration of fault-zone dilation, *Geology*, *27*(12), 1095–1098, doi:10.1130/0091-7613(1999)027<1095:FBACPM>2.3.CO;2.

Sharma, P., et al. (2000), PRIME lab AMS performance, upgrades and research applications, *Nucl. Instrum. Methods Phys. Res., Sect. B*, *172*, 112–123, doi:10.1016/S0168-583X(00)00132-4.

Snyder, G., and U. Fehn (2004), Global distribution of I-129 in rivers and lakes: Implications for iodine cycling in surface reservoirs, *Nucl. Instrum. Methods Phys. Res., Sect. B*, *223–224*, 579–586, doi:10.1016/j.nimb.2004.04.107.

Teichert, B. M. A., et al. (2005), Fluid sources, fluid pathways and diagenetic reactions across an accretionary prism revealed by Sr and B geochemistry, *Earth Planet. Sci. Lett.*, *239*(1–2), 106–121, doi:10.1016/j.epsl.2005.08.002.

Tomaru, H., et al. (2006), Effect of massive gas hydrate formation on the water isotopic fractionation of the gas hydrate system at Hydrate Ridge, Cascadia margin, offshore Oregon, *Geochem. Geophys. Geosyst.*, *7*, Q10001, doi:10.1029/2005GC001207.

Tomaru, H., et al. (2007a), Age variation of pore water iodine in the eastern Nankai Trough, Japan: Evidence for different methane sources in a large gas hydrate field, *Geology*, *35*, 1015–1018, doi:10.1130/G24198A.1.

Tomaru, H., et al. (2007b), Origin and age of pore waters in an actively venting gas hydrate field near Sado Island, Japan Sea: Interpretation of halogen and 129I distributions, *Chem. Geol.*, *236*, 350–366, doi:10.1016/j.chemgeo.2006.10.008.

Tomaru, H., et al. (2007c), Origin and age of pore waters in an actively venting gas hydrate field near Sado Island, Japan Sea: Interpretation of halogen and I-129 distributions, *Chem. Geol.*, *236*(3–4), 350–366, doi:10.1016/j.chemgeo.2006.10.008.

Torres, M. E., et al. (2004a), Relationship of pore water freshening to accretionary processes in the Cascadia margin: Fluid sources and gas hydrate abundance, *Geophys. Res. Lett.*, *31*, L22305, doi:10.1029/2004GL021219.

Torres, M. E., et al. (2004b), Gas hydrate growth, methane transport, and chloride enrichment at the southern summit of Hydrate Ridge, Cascadia margin off Oregon, *Earth Planet. Sci. Lett.*, *226*(1–2), 225–241, doi:10.1016/j.epsl.2004.07.029.

Trehu, A. M., et al. (2004), Three-dimensional distribution of gas hydrate beneath southern Hydrate Ridge: Constraints from ODP Leg 204, *Earth Planet. Sci. Lett.*, *222*(3–4), 845–862, doi:10.1016/j.epsl.2004.03.035.

Ullman, W. J., and R. C. Aller (1983), Rates of iodine remineralization in terrigenous near-shore sediments, *Geochim. Cosmochim. Acta*, *47*(8), 1423–1432, doi:10.1016/0016-7037(83)90301-0.

Wallmann, K., et al. (2006), Kinetics of organic matter degradation, microbial methane generation, and gas hydrate formation in anoxic marine sediments, *Geochim. Cosmochim. Acta*, *70*(15), 3905–3927, doi:10.1016/j.gca.2006.06.003.

Weinberger, J. L., and K. M. Brown (2006), Fracture networks and hydrate distribution at Hydrate Ridge, Oregon, *Earth Planet. Sci. Lett.*, *245*(1–2), 123–136, doi:10.1016/j.epsl.2006.03.012.